PAPER

Impact of tunable 2-(1*H*-indol-3-yl)acetonitrile based fluorophores towards optical, thermal and electroluminescence properties†

Subramanian Muruganantham, [ID] [a] Gunasekaran Velmurugan, [ID] ‡[a] Justin Jesuraj, [ID] [b] Hassan Hafeez,[b] Seung Yoon Ryu, [ID] *[b] Ponnambalam Venuvanalingam [ID] *[a] and Rajalingam Renganathan [ID] *[a]

Herein, we have synthesized 4,5-diphenyl-1*H*-imidazole and 2-(1*H*-indol-3-yl)acetonitrile based donor–π–acceptor fluorophores and studied their optical, thermal, electroluminescence properties. Both the fluorophores exhibit high fluorescence quantum yield (Φ_f = <0.6) and good thermal stability (T_{d10} = <300 °C), and could be excellent candidates for OLED applications. Moreover, the ground and excited state properties of the compounds were analysed in various solvents with different polarities. The geometric and electronic structures of the fluorophores in the ground and excited states have been studied using density functional theory (DFT) and time-dependent density functional theory (TDDFT) methods. The absorption of BIPIAN and BITIAN in various solvents corresponds to $S_0 \rightarrow S_1$ transitions and the most intense bands with respect to the higher oscillator strengths are mainly contributed by HOMO → LUMO transition. Significantly, the vacuum deposited non-doped OLED device was fabricated using BITIAN as an emitter, and the device shows electroluminescence (EL) at 564 nm, maximum current efficiency (CE) 0.687 cd A^{-1} and a maximum external quantum efficiency (EQE) of 0.24%.

Introduction

Elongated organic π-conjugated molecules are extensively used in making organic electronic materials due to their enormous potential applications[1] in two photon-absorption,[2] organic semiconductors,[3] organic photovoltaics (OPVs),[4] organic field effect transistors (OFET's),[5] information storage devices,[6] nonlinear optics (NLO),[7] sensors,[8] organic light emitting diodes (OLEDs),[9] *etc.*, and these systems show tunable optical and electrical properties. Owing to their promising applications in developing modern full-colour flat-panel displays and solid-state light sources, OLEDs have received considerable attention.[10] In the last few decades the vacuum thermal deposition process,[11] which is one of the important techniques, has been used for fabricating OLEDs. Since the invention[12] of multi-

layered OLEDs in 1987 by Tang and Van Slyke they are commonly used in many display applications.[13] Organic fluorophoric materials have been used to produce primary color red-green-blue (RGB) and near-infrared (NIR) emissions. The emission behaviour is usually tuned by conjugation, effective chromophores and dopants in hole–electron transporting materials.[14] The spin statistic rule suggested that the conventional[15] OLEDs can harvest 25% for internal quantum efficiency (IQE) due to the limited electron–hole conversion, and phosphorescence emitters can harvest both singlet–triplet excitons for the electroluminescence process.[16] Recently, Adachi and co-workers[17] developed thermally activated delayed fluorescence (TADF) technique using D–A (donor–acceptor) organic small molecules as emitters, which could harvest 100% IQE due to reverse intersystem crossing (RISC) process.[17a,b] In the p-i-n type fluorescence OLEDs the anode has injected hole through p-doped hole transporting layer (HTL) to the emissive layer and the cathode has injected electron *via* n-doped electron transporting layer (ETL) to the emissive layer leading to recombination of charge in the emissive layer which emits high efficient light.[18] Interestingly, organic small molecules incorporated with electron donor (D) and acceptor (A) by a linearly connected π-spacer exhibit special patterns in optical and electrical properties,[19] and such compounds have large electric dipoles in the excited states which also enhance intramolecular charge transfer (ICT).[20] Many D–A type organic small molecules have been used as luminogen in OLED applications. Among these,

aSchool of Chemistry, Bharathidasan University, Tiruchirappalli-620 024, Tamil Nadu, India. E-mail: venuvanalingam@yahoo.com; rrengas@gmail.com; Fax: +91-431-2407045; Tel: +91-431-2407053

bSchool of Display and Semiconductor Physics, Display Convergence, College of Science and Technology, Korea University, Sejong Campus 2511 Sejong-ro, Sejong City, 30019, Republic of Korea. E-mail: Justie74@korea.ac.kr

† Electronic supplementary information (ESI) available: Detailed photophysical properties, lifetime measurement, DSC curves, cyclic voltammogram, solvatochromism behaviour, theoretical study results and electroluminescence performance. See DOI: 10.1039/c8ra10448d.

‡ Present address: Institute of Inorganic Chemistry, Heidelberg University, Im Neuenheimer Feld 275, 69120 Heidelberg, Germany.

highly substituted imidazole derivatives received significant concern in developing novel luminogen materials for opto-electronic materials.[21] Small organic molecules having highly substituted imidazole moiety as an electron donor with various acceptors were scarcely reported.[22] Based on our knowledge, there is no literature available for 4,5-diphenyl-1H-imidazole linked 2-(1H-indol-3-yl)acetonitrile as luminogens. In this context, we planned to synthesize 4,5-diphenyl-1H-imidazole linked 2-(1H-indol-3-yl)acetonitrile and evaluate its thermal, optical, electrochemical stability and investigate the structure–property relationship of ambipolar π-conjugated luminogen materials. The D–π–A compound is probed as p-i-n type non-doped multilayer OLEDs to afford high efficient yellowish green emission (the CIE values of 0.45, 0.52). Further, the D–π–A interactions, optical and electrical properties are actually elucidated with a view to explore suitable candidates to develop multifunctional luminogen materials in the future.
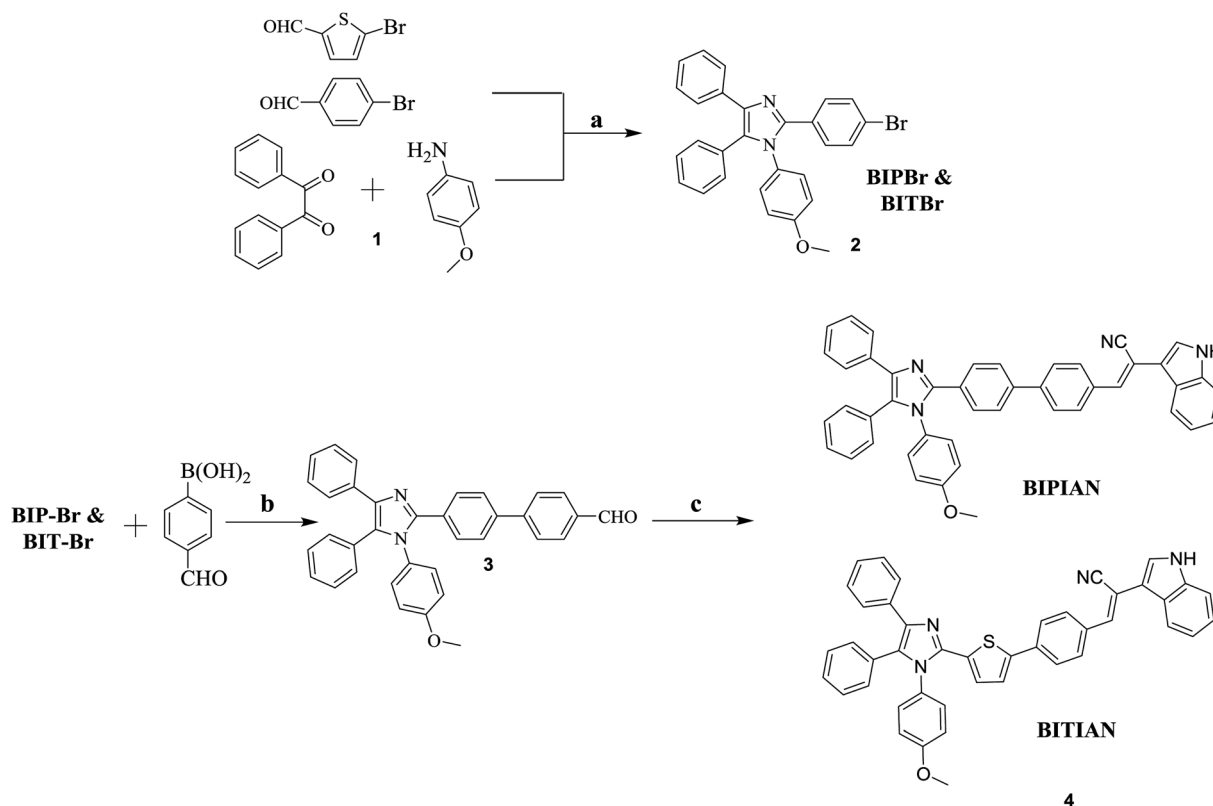
Results and discussion

Synthesis and characterization

The targeted molecule BIPIAN and BITIAN were designed and synthesized using various synthetic steps as illustrated in Scheme 1, the detailed synthetic procedure is described in the experimental part. The highly-substituted imidazole core was assembled via one-pot multi-component reaction[23] followed by the Suzuki cross-coupling reaction[24] to obtain the formyl group

incorporated imidazole. Finally, Knoevenagel condensation[25] of the corresponding aldehyde with 2-(1H-indol-3-yl)acetonitrile was carried out to afford the target molecules BIPIAN and BITIAN with good yield. In all the steps, the compound was purified by column chromatography (hexane/dichloromethane) using silica gel (100–200 mesh) and characterized using FT-IR, NMR and mass spectrometry.

Photophysical properties

The aim of this study is to understand the structure–property relationship of newly constructed imidazole based D–π–A organic small molecules. Generally, imidazole derivatives are widely used to build efficient fluorescent OLEDs due to their twisted structure and charge transporting ability. Indeed, the synthesized imidazole derivatives have better solubility in common organic solvents like dichloromethane, toluene, tetrahydrofuran, chloroform and N,N-dimethylformamide but poor solubility in methanol and water due to the presence of hydrophobic aromatic units with the concentration of 10^{-5} M. The steady-state optical behaviour of the emitters was investigated using ultraviolet-visible (UV-Vis) and photoluminescence spectrometry (PL) in both solution and solid films state on quartz substrate which is better to understand the photophysical properties. The key optical parameters are displayed in Table 1.

Scheme 1 Synthetic route for BIPIAN and BITIAN derivatives. Reaction conditions: (a) NH₄OAc, AcOH, 80 °C, 3 h; (b) 4-formylphenylboronic acid, Pd(PPh₃)₄, K₂CO₃, THF, water, 80 °C, 12 h; (c) indole-3-acetonitrile, ^{t}BuOK, MeOH, 75 °C, 3 h.

Table 1 Photophysical parameters for BIPIAN and BITIAN derivatives

Solvents	BIPIAN							BITIAN				
	$^a\lambda_{abs}$	$^b\varepsilon$	$^c\lambda_{emi}$	$^d\Phi_f$	^{e}Stokes shift	$^fE_T(30)$	λ_{abs}	ε	λ_{emi}	Φ_f	Stokes shift	$E_T(30)$
CyHex	406	10 696	476	0.40	3622	62.42	405	12 584	458	0.34	3858	60.06
Toluene	380	44 052	437	0.53	3432	60.31	412	105 842	474	0.53	3174	65.42
THF	382	62 992	463	0.38	4579	58.34	411	168 314	490	0.57	3922	61.75
DCM	376	198 882	476/539	0.40	5182	57.99	408	132 902	493/534	0.66	5783	60.06
CHCl$_3$	376	27 828	466	0.64	5136	58.11	408	118 876	492/530	0.69	5641	61.35
ACN	374	45 682	483	0.30	5685	57.87	404	159 550	494/537	0.23	6130	59.19
Acetone	379	60 322	479	0.31	5063	57.99	408	129 776	493/534	0.28	5748	59.68
DMF	385	104 156	480	0.23	5140	57.87	413	140 772	494/535	0.27	5521	59.56
MeOH	376	21 284	477	0.57	5631	57.99	402	70 560	493/534	0.42	6149	59.93
EtOH	379	22 622	476	0.36	5376	58.11	407	140 262	492/532	0.38	5773	60.06

^{a} Absorption (nm). ^{b} Molar absorption co-efficient (M^{-1} cm^{-1}). ^{c} Emission. ^{d} Fluorescence quantum yield (Φ_f). ^{e} Stokes shift (Δv cm^{-1}). ^{f} $E_T(30)$ (kcal mol^{-1}).

Absorption spectra

Fig. 1 shows UV-Visible absorption spectra of BIPIAN and BITIAN derivatives which exhibit similar absorption pattern at 270 nm with lower intensity than the π–π* transition of conjugated skeleton at 376 and 408 nm respectively. Fig. S1 and S3† show the absorption band in the range of 376–406 and 402–413 nm in various solvents for BIPIAN and BITIAN respectively and the longer wavelength bands can be attributed to π–π* transitions of imidazole donor and 2-(1H-indol-3-yl)acetonitrile acceptor unit. Notably, the absorption spectra are strong and broad which covers 350 to 450 nm for BIPIAN and 330 to 470 nm for BITIAN. Moreover, the intensity of π–π* transitions is higher than that of the charge-transfer transition. In addition, intramolecular charge transfer (ICT) transition was observed at 408 nm which occurs between D–A unit.[26] The optical energy gaps obtained from the onset of the absorption spectrum in dichloromethane solution are (E_g) 2.77 and 2.48 eV for BIPIAN and BITIAN respectively. Indeed, both fluorophores exhibit moderate to strong molar extinction coefficient (BIPIAN 1.90 and BITIAN 1.30 × 10^5 M^{-1} cm^{-1}) of D–π–A system. This is well supported by computational predictions.

Photoluminescence studies

The emission behavior of electronically excited molecules was investigated in dichloromethane (Fig. 1), to identify the solvent effect on the excited state. We observed most intense emission λ_{max} at 467 and 493 nm (excited at 376 and 408 nm) and a full width at half maximum (FWHM) of 69 and 99 nm for emitter BIPIAN and BITIAN respectively. In PL peaks, red-shift was observed in various solvents ranging from 437 to 483 and 458 to 494 nm for BIPIAN and BITIAN respectively. Indeed, the solvent-dependent excited state behaviour was observed in both compounds.[27]

The fluorescence quantum yields (Φ_f) of the highly-substituted imidazole derivatives were investigated in various solvents from non-polar cyclohexane to polar N,N-dimethylformamide. The observed quantum yields (Φ_f) lie in the range of 0.23–0.64 for BIPIAN and 0.23–0.69 for BITIAN (Table 1). However, the external quantum efficiency of thin film BITIAN estimated by the integrating sphere technique provides 0.24% of quantum yield. On the contrary, the fluorescence quantum yield decreased on increasing the solvent polarity implying intramolecular charge transfer of the excited state. In addition, the fluorescence quantum yield was observed in less polar solvents (i.e., CyHex, toluene, CHCl$_3$ and THF), which is higher than that of polar solvents (i.e., DCM, acetone, EtOH and MeOH). As well the more polar solvent such as, DMF and ACN show significantly lower fluorescence quantum yield. Obviously, the higher Stokes shift for BIPIAN and BITIAN leads to enhanced charge transfer at the locally excited state of the molecule. Among these, BITIAN shows larger Stokes shift due to the presence of thiophene π-spacer leading to a significant structural reorganization of the molecule. In PL emission behaviour, both the molecules show shoulder and peak in a polar solvent but no such thing was observed in non-polar solvents. Hence, the emission band strongly depended on the solvent polarity, which favours the occurrence of ICT under light excitation. The strong bathochromic shift was observed in both molecules due to the presence of highly conjugated units between imidazole and 2-(1H-indol-3-yl)acetonitrile. Noticeably, the solvatochromic study was performed to understand the
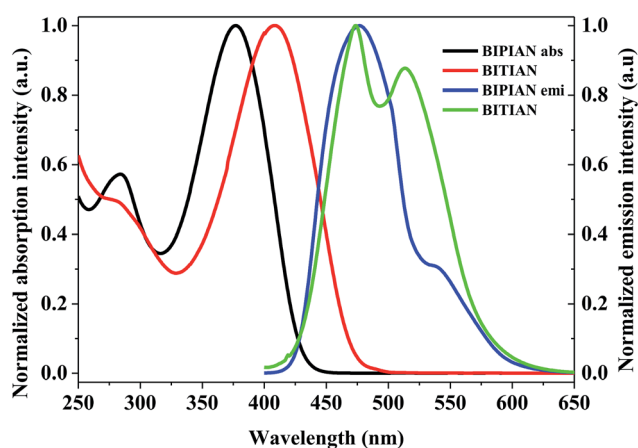

Fig. 1 Absorption/emission spectra for BIPIAN and BITIAN.

interaction of emitters with the solvent environment on the ground and excited state with various polarities of solvents implying a positive solvatochromism. Moreover, the positive solvatochromic emitters strongly induce the ICT behaviour on the excited state. Further, the ICT effect was distinguished by polarity of solvent and photoluminescence emission process (Fig. S2 and S4†).

The increasing solvent polarity from non-polar cyclohexane to polar N,N-dimethylformamide, enhanced the ICT character. Significantly, the absorption spectra were independent of solvent polarity while the emission spectra dependent. When the polarity of the solvent increases, the interaction between solvent and solute also increases which reveal more positive solvatochromism in emission spectrum as shown in Fig. 1. Probably, the emission spectra exhibit higher wavelength in polar solvents due to photoinduced intramolecular charge transfer, structural reorganization, dipole–dipole interaction and excimer complex formation, etc. Further, the observed Stokes shift values are listed in Table 1. The solvatochromic effect was investigated using Lippert–Mataga plot, Stokes shift versus orientation polarizability (Δf) of synthesized compounds, which describe the effect of solvent in the ground and electronically excited state of the molecule (Fig. S5 and S6†).[28]

Normally, the solvatochromism is related to the dipole moment of electronically excited and ground state of the molecule. The synthesized molecules examined for Stokes shift from the non-polar (CyHex) to polar solvent (DMF) and it revealed that a higher charge transfer character is observed. It is noted that the Stokes shift for BITIAN and BIPIAN falls in the range 3858–6149 cm^{-1} and 3622–5631 cm^{-1} respectively. The large Stokes shift observed for fluorophores indicate a higher dipole moment in the excited state than ground state. Interestingly, the large Stokes shifts for the emitters are more advantageous and favourable for electroluminescence devices, which may assist to avoid discarded self-absorptions. Solvatochromism behaviour was described in a well-known method by Reichardt–Dimroth polarity $E_T(30)$ parameters.[29] Correlation between Stokes shift versus $E_T(30)$ parameter indicates non-linearity in solvatochromism behavior (Fig. S7†). Due to the specific solvent effect divergence from linear dependence, may result from solute–solvent interactions and large difference in dipole–dipole (enhance the charge transfer) interactions in the excited state.[30]

Fluorescence lifetime measurement

The fluorescence decay time in the excited state of newly synthesized molecule was investigated using time-correlated single-photon counting technique.[31] Initially, the lifetime histogram was well fitted in single-exponential decay in dichloromethane solution exhibiting lifetime (τ) 1.08 and 1.12 ns for BIPIAN and BITIAN, respectively and the χ^2 values are calculated for BIPIAN is 1.01 and BITIAN is 2. Fig. S8† and 2 show fluorescence decay curves of BIPIAN and BITIAN, which is influenced by emission behaviour. Further, the solvent polarity varied from non-polar to polar (such as cyclohexane, DCM, ACN and MeOH), fluorescence decay was fitted to mono or bi-
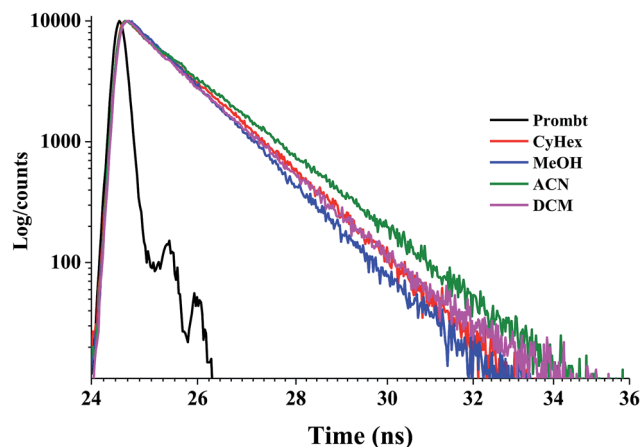

Fig. 2 Fluorescence decay curves of BITIAN in various solvents.

exponential decay based on the fitting ability. The fluorophores surrounded by solvent molecules and polarity of solvents leads to various intensity of decay which represents the conformational distribution of the lifetime. The steady-state measurement of fluorescence decay was observed for both molecules in different solvents which resulted in bi-exponential decay (lifetime-weighted quantum yield or amplitude-weighted lifetime). Further, the average lifetime $\langle \tau \rangle$ was calculated and the detailed fluorescence decay measurements data are listed in Table S1.†

Two distinct lifetimes were observed for a single fluorophoric compound which indicates bi-exponential decay of electronically excited state. Bi-exponential decay may arise due to various conformations of the excited molecule, solvent effect, molecular environment and dissimilar spin-multiplicities of the excited state. Subsequently, internal PL quantum yield (Φ_{PL}) and average fluorescence decay lifetime were used to calculate radiative (k_r) and non-radiative (k_{nr}) decay using corresponding equation[32] and results are summarized in Table S1.† Significantly, the Φ_{PL} was obtained for both molecules which illustrated a higher radiative rate constant due to the presence of electron withdrawing units thus enhancing the intersystem crossing and internal conversion in the ground state. BIPIAN in acetonitrile shows non-radiative decay and this may be due to the interaction between solvent–solute. Based on these results, both luminogen molecules are suitable for OLEDs applications.

Optimized geometry and frontier molecular orbital analysis

The C–C bond lengths in BIPIAN and BITIAN fall in between their respective single and double bond limits and this indicates the C–C bond present in both molecules is no longer a pure single bond (due to delocalization of π-electrons).[21b,23,33] Similarly C–N, C–O and C–S bond lengths also are lower than its actual bond lengths. This also shows an enhanced delocalization of π-electrons due to co-planarity of the benzene and thiophene rings in the molecule (Fig. S9 and S10†). The highest occupied molecular orbitals (HOMOs), lowest unoccupied molecular orbitals (LUMOs) and band gaps (HOMO–LUMO gap) of BIPIAN and BITIAN have been explored to recognize the

nature of electronic and optical properties.[34] It is interesting to note that the HOMO of BIPIAN is localized mainly on the substituted imidazole and phenyl ring while the LUMO is mainly centered on the phenyl ring and 2-(1H-indol-3-yl)acetonitrile units. On the other hand, HOMO−1, HOMO−2, HOMO−3, LUMO+1 and LUMO+2 orbitals are predominantly localized on the substituted imidazole while the LUMO+3 of BIPIAN is localized on the substituted imidazole and 2-(1H-indol-3-yl)acetonitrile and phenyl unit (Fig. 3). The HOMO of BITIAN is equally localized on the highly-substituted imidazole and thiophene ring while the LUMO is centered on the entire molecule (highly-substituted imidazole, phenyl or thiophene ring and 2-(1H-indol-3-yl)acetonitrile). The HOMO−1 and HOMO−2 of BITIAN are principally localized on the highly-substituted imidazole whereas HOMO−3 is primarily distributed on the 2-(1H-indol-3-yl)acetonitrile. However, LUMO+1, LUMO+2 is centred on the highly-substituted imidazole and LUMO+3 is centered on the 2-(1H-indol-3-yl)acetonitrile (Fig. 3).
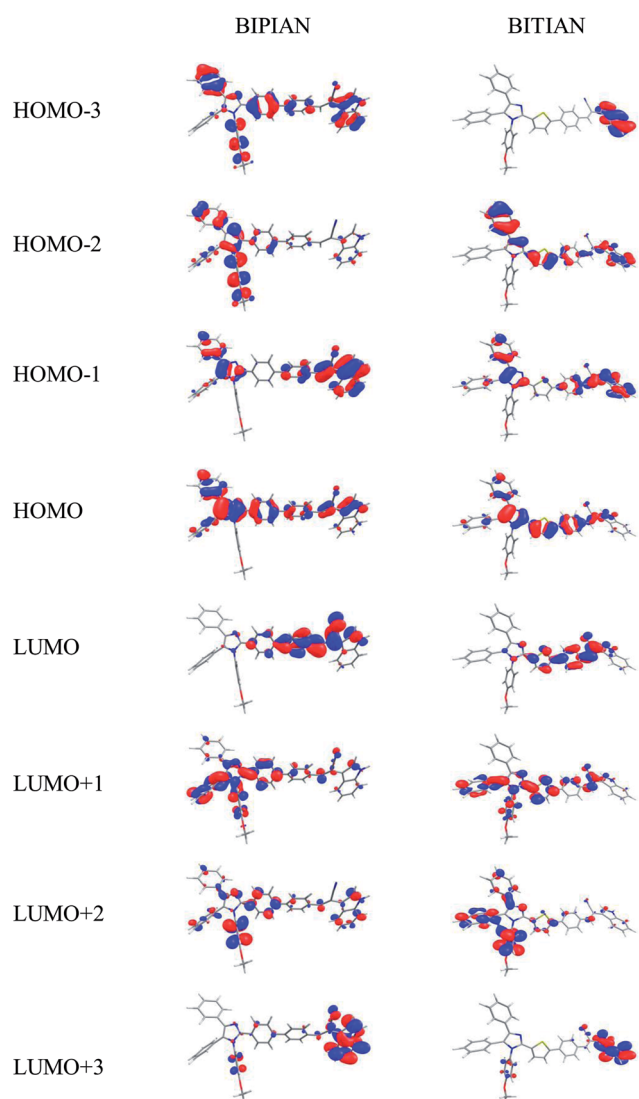

Fig. 3 Calculated frontier molecular orbitals of the BIPIAN and BITIAN at the B3LYP/6-31G+(d,p) level.

This signifies that the HOMO → LUMO transition bears a significant ICT and π → π* character and the other absorption bands have dominant contributions from HOMO−1 → LUMO and are mainly π → π* character. The energy gaps of compounds BIPIAN and BITIAN are found to be 3.18 and 2.91 eV respectively (Fig. 4). The HOMO levels for BIPIAN and BITIAN are observed at −5.39, −5.18 eV, respectively. The LUMO levels for them are in the range of −2.21 and −2.27 eV (Fig. 3) for BIPIAN and BITIAN respectively. Both compounds are compared with the Mes₂B[p-4,4′-biphenyl-NPh(1-napthyl)] (BNPB) due to their wider usability as HTM in OLEDs. The HOMO of BIPIAN (−5.39 eV) and BITIAN (−5.18 eV) is comparable with BNPB (Exp. = −5.30 eV;[35] −5.27 eV at b3lyp/6-311g(d,p) by DFT calculations).[33a] The LUMO levels of BIPIAN (−2.21 eV) and BITIAN (−2.27 eV) are comparable with that of BNPB (Exp. = −2.44 eV; 1.88 eV at b3lyp/6-311g(d,p) level). Interestingly, the HOMO level of BIPIAN and BITIAN are slightly higher than the work function of the Indium Tin Oxides (ITO; from −4.8 to −5.1 eV),[36] and the LUMO levels are higher than that of the tris(8-hydroxyquinoine)aluminium (Alq₃, −1.81 eV),[37] which is one of the widely used electron transport material. This indicates that BIPIAN and BITIAN can act as 'tri-functional materials' (emitter, hole and electron transporters) in OLEDs.

To understand the nature of various segments of the molecule and their individual contributions towards HOMOs and LUMOs (using QMForge[38]), the whole molecule has been segmented into three fragments, namely donor (imidazole), π-spacer (phenyl or thiophene ring) and acceptor units (2-(1H-indol-3-yl)acetonitrile). As evident from the molecular orbital diagrams, HOMOs of BIPIAN are mainly centralized by the donor (56%) and π-spacer (30%) and interestingly LUMOs are majorly stabilized by π-spacer (54%) and acceptor (25%). The donor part contributes majorly on the HOMO−1 (53%), HOMO−2 (88%), HOMO−3 (78%), LUMO+1 (56%), LUMO+2 (91%) and LUMO+3 (43%). In the case of BITIAN, the HOMO is equally contributed by the donor (40%) and π-spacer (47%). The HOMO−1 (57%), HOMO−2 (81%), LUMO+1 (67%) and LUMO+2 (90%) are majorly contributed by donor part and HOMO−3 (73%) and LUMO+3 (49%) located on acceptor units (Table 2). This confirms that the donor and acceptor parts in BIPIAN and BITIAN are responsible for the intramolecular charge transfer upon excitation.

To understand the nature of electronic transitions and contributing configurations of BIPIAN and BITIAN, TD-DFT calculations on the absorption and emission in both vacuum and in solvent (with various solvents) were performed. The calculated absorption spectrum of BIPIAN and BITIAN are in good agreement with the experimental results (Table S2†). The electronic transitions are of the π → π* character, and excitation to S₁ state corresponds exclusively to the promotion of an electron from HOMO → LUMO (67–84%). The experimental band in toluene is found at 380 nm for BIPIAN corresponds to the transition predicted at 371 nm, and this originates from HOMO → LUMO transition with π → π* transition character (80%). The experimental band predicted in THF at 382 nm corresponds to the transition calculated at 373 nm with larger
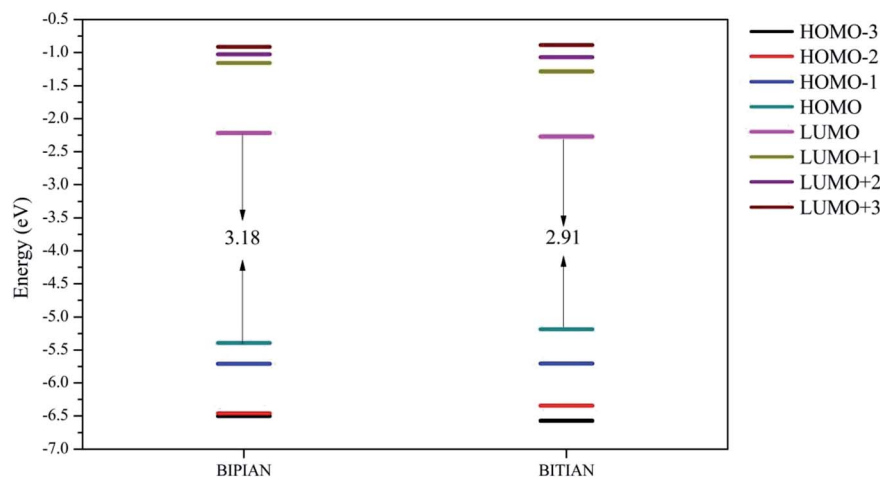
Fig. 4 Molecular orbital energy level graphs of BIPIAN and BITIAN at the B3LYP/6-31G+(d,p) level.

Table 2 Frontier molecular orbital compositions (%) in the ground state for BIPIAN and BITIAN at the B3LYP/6-31G+(d,p) level

	Orbital	Contribution (%)		
		Donor	π-Spacer	Acceptor
BIPIAN	HOMO−3	78.29	14.59	7.12
	HOMO−2	88.26	7.64	4.10
	HOMO−1	52.56	24.39	23.05
	HOMO	55.73	29.52	14.76
	LUMO	21.40	53.72	24.88
	LUMO+1	55.73	33.96	10.30
	LUMO+2	90.56	4.83	4.60
	LUMO+3	42.66	6.44	50.90
BITIAN	HOMO−3	2.82	23.67	73.51
	HOMO−2	80.83	13.08	6.09
	HOMO−1	56.27	22.56	21.17
	HOMO	40.21	47.21	12.58
	LUMO	50.32	29.37	20.31
	LUMO+1	67.09	11.44	21.47
	LUMO+2	90.33	5.73	3.94
	LUMO+3	37.30	13.56	49.15

oscillator strengths which originate from HOMO → LUMO (77%) with π → π* character. In DCM and CHCl$_3$, the experimental band found at 376 nm corresponds to the transition calculated at 371 and 372 respectively. This transition has significant π → π* character due to the exclusive promotion of an electron from HOMO → LUMO (74–77%). Similar trend was observed in ACN, acetone, DMF, MeOH and EtOH and the excitations correspond to S$_1$ state exclusively to the promotion of an electron from HOMO → LUMO (67–84%) with significant π → π* character. For BITIAN, the experimental band in cyclohexane found at 405 nm corresponds to the transition computed at 405 nm and it originates mainly to the excitation to S$_1$ states from HOMO → LUMO (81%) with significant π → π* character. The experimental band predicted in toluene at 412 nm, corresponds to the transition calculated 407 nm with larger oscillator strengths which originates from HOMO → LUMO (81%) with π → π* character. In THF and DCM, the

experimental bands found at 411 and 408 nm, corresponds to the transition calculated at 407 nm for both solvents. This transition has significant π → π* character due to the exclusive promotion of an electron from HOMO → LUMO (83%). The same has been observed in CHCl$_3$, ACN, acetone, DMF, MeOH and EtOH and the excitations are to S$_1$ state and is mainly contributed by HOMO → LUMO transition (83–84%) and it has significant π → π* character. In comparison with gas phase simulated absorption spectra, the solvent phase spectra shows red shift due to the solute–solvent interaction.[39] Overall, the absorption of BIPIAN and BITIAN with various solvents corresponds to S$_0$ → S$_1$ transitions and the most intense bands with higher oscillator strengths are mainly contributed by HOMO → LUMO transition (67–84%) of significant π → π* character.

Theoretical emission spectra for BIPIAN and BITIAN based on optimized excited-state geometries are presented in Table 3. The emission peaks in THF solvent for BIPIAN, with the largest oscillator strength are due to LUMO → HOMO transition (93%). The emission peaks in toluene, DCM, CHCl$_3$ and ACN with the largest oscillator strength for the BIPIAN are assigned to π → π* character, arising from the HOMO → LUMO transition (~93%). The calculated values of fluorescence wavelength are located at 450, 452, 451 and 451 nm which correspond to the experimental values found at 437, 476, 466 and 483 nm respectively. The emission peaks in cyclohexane for BITIAN with the largest oscillator strength arises from LUMO → HOMO transition (92%). The emission peaks in toluene, THF, DCM, CHCl$_3$ and ACN with the largest oscillator strength for BITIAN are assigned to π → π* transition arising from the HOMO → LUMO transition (93–94%). The calculated values of fluorescence wavelength are located at 467, 467, 467, 467 and 467 nm which correspond to the experimental values obtained at 474, 490, 493, 492 and 493 nm respectively. The same trend has been observed in acetone, DMF, MeOH and EtOH. The highest oscillator strengths of the S$_1$ → S$_0$ transition for BIPIAN and BITIAN imply that they have a large fluorescent intensity and are useful as fluorescent OLED materials. The influence of various solvents on the emission spectra was simulated by using PCM.

Table 3 Computed emission spectra in both gas and solvent phase BIPIAN and BITIAN along with experimental data

Molecule	States	Electron transition	Cal. λ_{max} (nm)	Exp. λ_{max} (nm)	Oscillator strength (f)	E (eV)	E_b (eV)	Major contribution	τ (ns)
BIPIAN	Gas-phase	$S_1 \rightarrow S_0$	425.9	—	1.613	2.91	0.27	HOMO $\rightarrow$ LUMO (93%)	1.69
	CyHex	$S_1 \rightarrow S_0$	447.7	476	1.658	2.77	0.41	HOMO $\rightarrow$ LUMO (93%)	1.81
	Toluene	$S_1 \rightarrow S_0$	450.5	437	1.658	2.75	0.43	HOMO $\rightarrow$ LUMO (93%)	1.84
	THF	$S_1 \rightarrow S_0$	451.2	463	1.620	2.75	0.43	HOMO $\rightarrow$ LUMO (94%)	1.88
	DCM	$S_1 \rightarrow S_0$	452.2	476	1.619	2.74	0.44	HOMO $\rightarrow$ LUMO (94%)	1.89
	CHCl$_3$	$S_1 \rightarrow S_0$	451.5	466	1.633	2.75	0.43	HOMO $\rightarrow$ LUMO (94%)	1.86
	ACN	$S_1 \rightarrow S_0$	450.8	483	1.599	2.75	0.43	HOMO $\rightarrow$ LUMO (94%)	1.90
	Acetone	$S_1 \rightarrow S_0$	451.0	479	1.604	2.75	0.43	HOMO $\rightarrow$ LUMO (94%)	1.90
	DMF	$S_1 \rightarrow S_0$	453.7	480	1.608	2.73	0.45	HOMO $\rightarrow$ LUMO (94%)	1.92
	MeOH	$S_1 \rightarrow S_0$	450.2	477	1.597	2.75	0.43	HOMO $\rightarrow$ LUMO (94%)	1.91
	EtOH	$S_1 \rightarrow S_0$	451.2	476	1.602	2.75	0.43	HOMO $\rightarrow$ LUMO (94%)	1.90
BITIAN	Gas-phase	$S_1 \rightarrow S_0$	447.0	—	1.863	2.78	0.13	HOMO $\rightarrow$ LUMO (92%)	1.60
	CyHex	$S_1 \rightarrow S_0$	465.2	458	1.976	2.67	0.24	HOMO $\rightarrow$ LUMO (91%)	1.63
	Toluene	$S_1 \rightarrow S_0$	467.5	474	1.986	2.65	0.26	HOMO $\rightarrow$ LUMO (92%)	1.65
	THF	$S_1 \rightarrow S_0$	466.9	490	1.968	2.66	0.25	HOMO $\rightarrow$ LUMO (92%)	1.65
	DCM	$S_1 \rightarrow S_0$	467.6	493	1.971	2.65	0.26	HOMO $\rightarrow$ LUMO (92%)	1.66
	CHCl$_3$	$S_1 \rightarrow S_0$	467.5	492	1.975	2.65	0.26	HOMO $\rightarrow$ LUMO (92%)	1.66
	ACN	$S_1 \rightarrow S_0$	465.9	494	1.955	2.66	0.25	HOMO $\rightarrow$ LUMO (92%)	1.66
	Acetone	$S_1 \rightarrow S_0$	466.2	493	1.958	2.66	0.25	HOMO $\rightarrow$ LUMO (92%)	1.66
	DMF	$S_1 \rightarrow S_0$	468.5	494	1.969	2.65	0.26	HOMO $\rightarrow$ LUMO (92%)	1.67
	MeOH	$S_1 \rightarrow S_0$	465.4	493	1.952	2.66	0.25	HOMO $\rightarrow$ LUMO (92%)	1.67
	EtOH	$S_1 \rightarrow S_0$	466.3	492	1.958	2.66	0.25	HOMO $\rightarrow$ LUMO (92%)	1.66

The results reveal that the emission wavelengths, coefficients and configurations are nearly identical for BIPIAN and BITIAN but a 3–20 nm red-shift has been observed and this is due to the solute–solvent interaction. The calculated absorption and emission bands are in good agreement with the experimental results. Overall, the DFT and TD-DFT calculations reveal deeper insights into the electronic structures, and optical properties and the nature of the transition of BIPIAN and BITIAN are well explored by theoretical methods.

The radiative lifetime (τ) have been computed for spontaneous emission.[40] OLED molecules with short radiative lifetime have been known to have high light-emitting efficiency while those with long radiative lifetime facilitate electron and energy transfer and the attack of active species.[41] Both BIPIAN and BITIAN show short radiative lifetime (1.63–1.92 ns) and this indicates that they are good light-emitting materials (Table 3). It is a key point toward the development of this type of materials for OLEDs. It is well-known that fluorescence emission is accompanied by energy ejection. When the energy of the fluorescence excitation is E_{Flu} and the energy difference between the HOMO and LUMO are ΔE_{H-L}, the exciton binding energy can be defined as $E_b = \Delta E_{H-L} - E_{Flu}$. Therefore the exciton binding energy (E_b) is the energy required to destroy a hole–electron exciton. The values of E_b for BIPIAN and BITIAN indicate that the energy required to destroy a hole–electron exciton follows the order BITIAN < BIPIAN.

Electrochemical properties

The redox property of the new fluorophores was probed using cyclic voltammetry, further the frontier molecular orbital level also studied. The results are shown in Fig. 5 and S11†, which indicate their potential application in bipolar charge transport material. The redox potential is a highly essential parameter for luminescent materials accordingly the hole/electron-injecting barrier was reduced. The imidazole derivatives exhibit similar reversible oxidation peak potential and detailed data was compiled in Table 4. The HOMO energy level was determined using the following formula: HOMO = (4.8 eV + E_{ox}), where, E_{ox} is onset oxidation peak potentials. Besides, the band gap energy (ΔE_g) of the molecules were examined from the onset wavelength which is obtained from intersecting of absorption and emission spectra, further which could be useful for calculating LUMO energy levels (LUMO = HOMO + ΔE_g). The HOMO energy levels for BIPIAN −5.75 eV, BITIAN −5.76 eV and LUMO energy level for BIPIAN −2.77 eV, BITIAN −2.48 eV. Intriguingly, the electrochemical stability of D–π–A compounds is evaluated using CV in dichloromethane by applying different scan rate from 100–1000 mV s^{-1} in repeated cycles. Hence, there is no
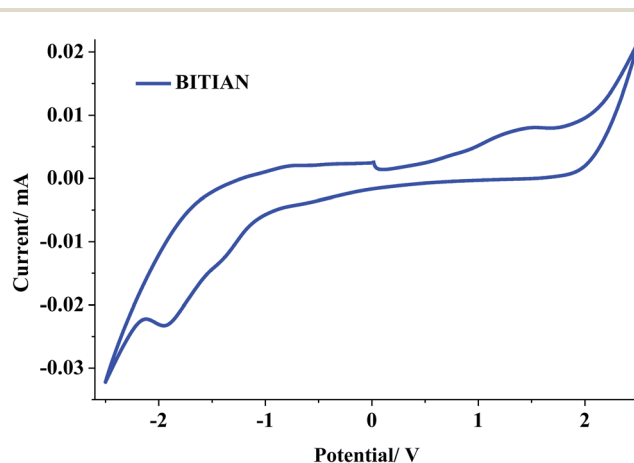
Fig. 5 Cyclic voltammogram of BITIAN.

Table 4 Photophysical, electrochemical, thermal data for BIPIAN and BITIAN compounds

Compounds	$^a\lambda_{abs}$	λ_{emi}	$^bE_{ox}$ [V]	^{c}HOMO [eV]	LUMO [eV]	E_g [eV]	^dT_g [°C]	T_{d10} [°C]	T_m [°C]	T_c [°C]
BIPIAN	376	476/539	1.45	−5.75	−2.98	2.77	253	318	283	185
BITIAN	408	493/534	1.46	−5.76	−2.98	2.48	384	312	n.d	n.d

^{a} Abs/emis maximum for both molecules. ^{b} Obtained from CV measurements in 1,2-dichloromethane solution. ^{c} The HOMO and LUMO energies were determined from CV and the absorption onset. Ferrocene (Fc; 4.8 eV) was used as the internal standard in each experiment. The Fc oxidation peak potential was located at +410 mV, relative to the saturated Ag/AgCl reference electrode. Evaluate from the onset of the absorption spectra, $E_g = (1240/\lambda_{onset})$. ^{d} Measured for T_g & T_d; (*i.e.* not detect).

change in the peak potential which revealed that both molecules are electrochemically more stable. It indicates that the energy levels are beneficial to assign superior electrochemical stability in optoelectronic device operation.

Thermal analysis

Thermal behaviour of synthesized D–π–A compounds was evaluated by thermogravimetric analysis (TGA) and differential scanning calorimetry (DSC) under nitrogen atmosphere with the heating rate of 10 °C min⁻¹. The TGA shown in Fig. 6 reveals that both compounds have good thermal stability although small molecular weight. We observed a higher onset decomposition temperature (T_d) at 308, 312 °C with 10% of weight loss and onset glass transition temperature (T_g) at 253, 384 °C for BIPIAN, BITIAN respectively. For BIPIAN, crystallization temperature observed at 185 °C and melting temperature at 283 °C but in the case of BITIAN unable to detect (Fig. S12† and Table 4). The thermal properties of biphenyl compounds are flexible in nature and have lower T_g/T_d of BIPIAN, when compared with BITIAN. Moreover, thermal behaviour of synthesized compounds was studied with better understanding and identified which is suitable to make uniform film morphology and an appreciable device performance.

Ionization potential, electron affinity and reorganization energy

To understand the nature of energy barrier for injection and transport rates for holes and electrons, we have computed

Fig. 6 Thermogravimetric analysis of BIPIAN and BITIAN.

ionization potentials (IPs), electronic affinities (EAs) and reorganization energies (λ) of BIPIAN and BITIAN.[42] The IPs and EAs, together with the hole extraction potential (HEP), which is the energy difference from M^+ (cationic) to M (neutral molecule) using the M^+ geometric structure and the electron extraction potential (EEP), which is the energy difference from M^- (anionic) to M using the M^- geometric structure. The IPs and EAs can be either for vertical excitations (v, at the geometry of the neutral molecule) or adiabatic excitations (a, at the optimized structures for both the neutral and charged molecule). The reorganization energies for electron transport ($\lambda_{electron}$) and hole transport (λ_{hole}) have been well clarified.[33,34d,43]

The main challenge for the application of organic molecules in OLEDs is the achievement of high EA and low IP to improve the electron and hole transport electronic devices.[33,44] For OLED material, lower the IP easier the entry of hole from indium tin oxide (ITO) to hole transporting layer (HTL) and higher the EA easier the entry of electron from cathode to electron transport layer (ETL).[45] It has been experimentally proved that BNPB is a good trifunctional molecule.[32,45] The IPs of BIPIAN (6.33 eV) and BITIAN (6.15 eV) are close to that of BNPB (6.09 eV), therefore they can be used as HTL materials. From EAs values, BIPIAN (1.07 eV) and BITIAN (1.17 eV) are expected to accept the electron easily than BNPB (0.74 eV).[46] Therefore both BIPIAN and BITIAN exhibit more excellent properties as ETL materials than BNPB due to the nature of donor and acceptor groups. The trends in the IPs and EAs of BIPIAN and BITIAN are similar to those of the negative HOMO and LUMO energies (Table S3†). To be an emitting layer material, it needs to achieve a balance between hole injection and electron acceptance. By theoretical concept, if λ value is lower, the charge-transport rate will be higher. The λ_{hole} for BIPIAN (0.27 eV) and BITIAN (0.28 eV) are lower than their respective $\lambda_{electron}$ (BIPIAN = 0.36 eV; BITIAN = 0.32 eV) and hence suggesting that the hole transfer rate is higher than the electron transport rate. Hence, these compounds can be used as an HTL than the ETL. However, the energy differences between the λ_{hole} and $\lambda_{electron}$ is very small about 0.09 and 0.04 eV for the compounds BIPIAN and BITIAN, thus these compounds can also act as ambipolar material.

Electroluminescence performance

The synthesized luminogen molecule BITIAN is fabricated as emissive layer in OLED device. Computed data indicates that these materials are suitable for both hole as well as electron transporting layer. Further, we plan to understand the emission properties of newly assembled D–A molecule using
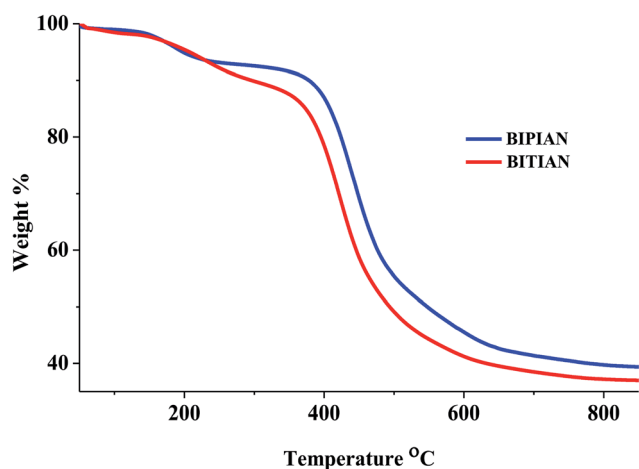
luminescence behaviour. Fig. 7 and S13† demonstrates the current density–voltage–luminance (J–V–L) plot of OLED containing BITIAN as emissive layer. The OLED structure consists of p-i-n configuration, where p denotes N,N'-di(1-naphthyl)-N,N'-diphenyl-(1,1'-biphenyl)-4,4'-diamine (NPB) as a HTL, n indicates 2,2',2''-(1,3,5-benzinetriyl)-tris(1-phenyl-1-H-benzimidazole) (TPBi) as ETL and i depicts the BITIAN layer. The exact configuration is as follows: ITO/NPB (40 nm)/BITIAN (40 nm)/TPBi (20 nm)/LiF/Al. The applied turn-on voltage of the device is 7.5 V indicating balanced electron to hole injection barrier available in this structure. However, the high hole injection barrier available at ITO/NPB as compared to electron injection may be a reason for this slightly higher turn-on voltage, the device working with an extended operating voltage up to 20 V. The lower luminance might attribute to the poor hole injection in to the BITIAN molecule. Because, deeper HOMO level of BITIAN (~5.7 eV) is expected to generate hole accumulation at BITIAN/TPBI interface owing to high injection barrier. As a result, we expected a larger electron leakage from the EML which subsequently reduced the luminance and device

performances. We speculated that with proper hole injection layers, this leakage problem can be reduced. The maximum luminance efficiency was observed around 100 cd m^{-2} at 20 V. Deep HOMO level of BITIAN is expected to generate electron accumulation at BITIAN/TPBI interface owing to high injection barrier for holes. After 7.5 V, the recombination process is started in BITIAN in which certain leakage current is contributed by the electron accumulations. To avoid this kind of leakage current, it is advisable to use hole injection layers. However, the emission achieved in this structure is only from BITIAN material.

The EL spectrum recorded at 11 V for the above-discussed OLED is depicted in Fig. 8. Hence the full width at half maximum (FWHM) for electroluminescence spectrum signifies the high color purity based on performance of the device. However, the maximum emission occurred at 564 nm and there is no additional peak observed. It indicates the charge
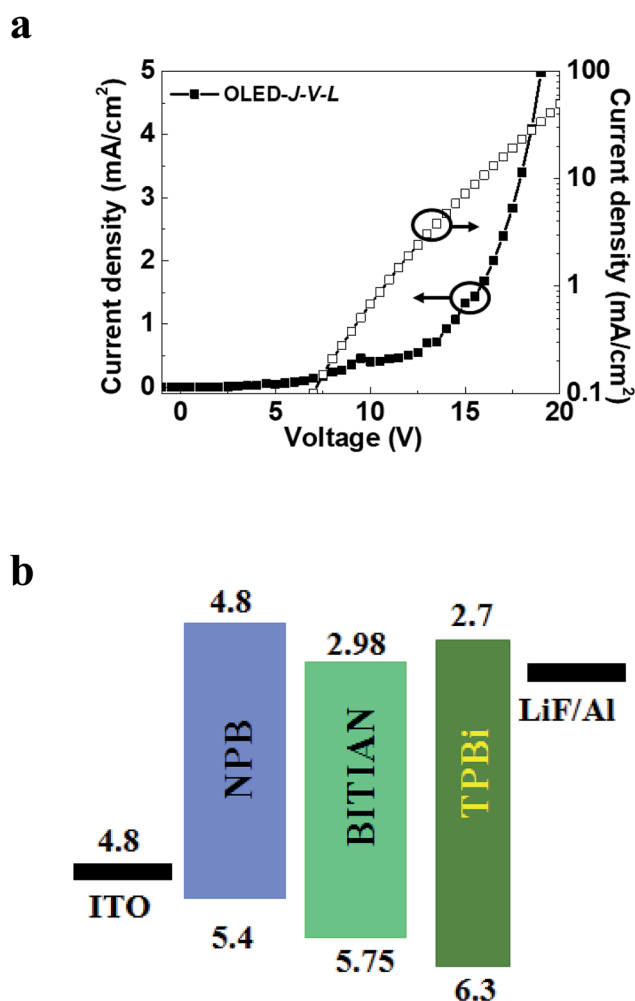

Fig. 7 (a) Current density (J)−voltage (V)−luminance (L) characteristics of p-i-n fluorescent OLED with BITIAN as emitting material and (b) schematic of the p-i-n OLED structure.
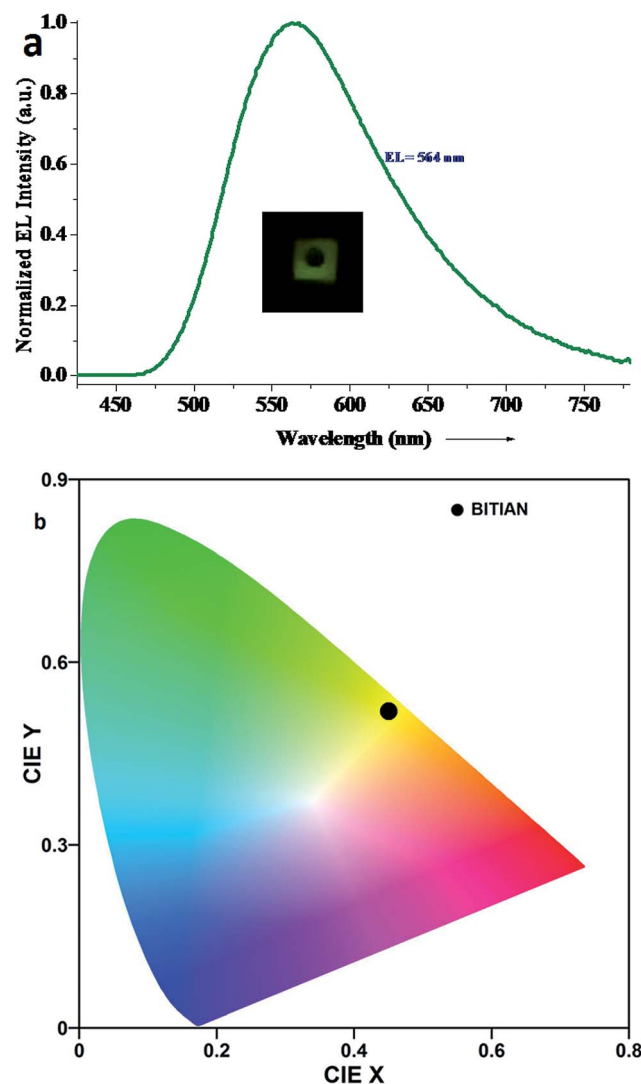

Fig. 8 (a) EL spectrum of p-i-n non-doped fluorescent OLEDs with BITIAN as emitting material and (b) CIE color coordinates of BITIAN with the NTSC standard.

Table 5 Electroluminescence performance for BITIAN

Device configuration	EL λ_{max} (nm)	FWHM λ_{max} (nm)	Turn on voltage (eV)	Maximum current efficiency cd A^{-1}	Maximum power efficiency (lm W^{-1})	Maximum quantum efficiency (%)	CIE 1931 Coordinates (x, y)
p-i-n type: (ITO/NPB/BITIAN/TPBI/ LiF/Al)	564	116	7.5	0.687	0.125	0.243	0.45, 0.52

recombination only generated on the BITIAN layer. The EL emission was observed at a longer wavelength (564 nm) than PL emission (534 nm). This kind of Stokes shift might be attributed to the charge traps presented in BITIAN due to certain oxidized species or due to the excimer formation.

Table 5 indicated the overall performance of p-i-n type non-doped fluorescent OLEDs using BITIAN as the emission layer. The CIE 1931 coordinates for this emission is found to be (x, y) 0.45, 0.52 indicating the yellowish green emission[47] thus confirms the photon generation only from the BITIAN. The maximum current and power efficiencies are 0.68 cd A^{-1} and 0.12 lm W^{-1} respectively. The EQE of the device reordered to be 0.24%. The relatively poor performances recorded for the above OLED might be attributed to the deep HOMO of BITIAN, which can contribute to leakage current by electron accumulation at ETL side. Even though, luminance is lower, the uniformity of the pixel was notably good as shown in the inset of Fig. 8. Further, the stability of the pixels also stable for under epoxy encapsulation for few days. However, the present work delineated the possibility of light generation with BITIAN compounds. Despite the poor performances, BITIAN proved to be an electroluminescence active material for OLED applications. CIE co-ordinates, emission wavelength and efficiencies reflected that the BITIAN can be processed in OLED as a fluorescent emitter material with a proper device configuration.

Conclusion

In summary, we have developed a new series of ambipolar type imidazole based D–π–A moiety with diverse linkage. The newly synthesized molecules (BIPIAN and BITIAN) are well characterized by various analytical techniques. The photophysical and electrochemical studies show that the synthesized fluorophores are compatible for OLED application. Further, both molecules have good thermal, morphological stability, larger Stokes shift, fluorescence quantum yield and enhanced charge balance abilities. In addition, Lippert–Mataga and $E_T(30)$ relationship suggest an increase of TCI in electronically excited molecules. We have also performed theoretical investigation to explore their optical, electronic properties, and device performance. The HOMO and LUMO levels of BIPIAN and BITIAN are compared with those of BNPB, ITO and Alq$_3$ and the results revealed that BIPIAN and BITIAN could be used as 'tri-functional materials' (emitter, hole and electron transporters) in OLEDs. Synthesized molecules were found to be efficient with the lowest band gap and high wavelength absorption and emission. The longest wavelength absorption corresponds to the excitation to the lowest singlet excited state, where the

electronic transitions are of $\pi \rightarrow \pi*$ type and excitation to S$_1$ state corresponds mainly to the promotion of an electron from HOMO $\rightarrow$ LUMO in BIPIAN and BITIAN. The λ_{hole} values of the BIPIAN and BITIAN are smaller than that of $\lambda_{electron}$ values and this suggests that the hole-transfer rate is better than the electron transfer rate. However, the energy differences between the λ_{hole} and $\lambda_{electron}$ is very small about 0.09 and 0.04 eV respectively for the compounds BIPIAN and BITIAN, and this indicates that these compounds can also act as ambipolar material. Indeed the results are encouraging and also in good agreement with EL performance of p-i-n type non-doped OLEDs. The emitter BITIAN molecule exhibits FWHM at 116 nm through EL spectrum of non-doped multi-layered device performance. The device reveal yellowish green emission with maximum EQE 0.26% and CE 0.687 cd A^{-1} under vacuum deposited process. BITIAN achieved a stable yellowish green EL at 564 nm and CIE coordinate (0.45, 0.52) conforming to NTSC standard.

Experimental section

General information

Materials and methods. All reagents were obtained from commercial sources, unless otherwise specified. The solvents toluene and tetrahydrofuran were purified by standard purification techniques. 4-Methoxyaniline, benzile, 4-formylphenylboronicacid, 4-bromobenzaldehyde, 5-bromo-2-thiophenecarboxaldehyde and 3-indoleacetonitrile were purchased from Sigma Aldrich or Alfa Aesar and used as received without further purification. All the reactions were conducted in oven-dried glassware under a positive pressure of argon with magnetic stirring. ^{1}H and ^{13}C NMR spectra were recorded (400 and 100 MHz, respectively) on a Bruker Avance DPX 400 MHz using CDCl$_3$ & DMSO-d$_6$. Chemical shifts for proton and carbon resonances are reported for the major isomer in parts per million (δ) relative to tetramethylsilane (δ 0.00), chloroform (δ 77.23) and DMSO-d$_6$ (δ 39.51), respectively. Multiplicities are indicated by singlet (s), doublet (d), triplet (t), multiplet (m). Coupling constants (J) were reported in hertz (Hz). Carbon types were determined from ^{13}C NMR and DEPT experiments. High resolution mass analyses were performed using electron spray ionization (ESI) technique on a Thermo Exactive Orbitrap mass spectrometer. Steady-state spectroscopic techniques were analyzed to obtain solution and film forming (JASCO V-360 spectrophotometer) by vacuum (2×10^{-6} mbar) deposition on a quartz substrate. UV/Vis absorption spectra were measured in various solvents such as spectroscopic or HPLC grade and photoluminescence (PL) spectra in solution were obtained on a JASCO FP-8300 spectrofluorometer

in different solvents (cyclohexane to *N,N*-dimethylformamide) performed at room temperature and the film was examined by using a JASCO V-630 spectrofluorometer respectively. Fluorescence quantum yield (Φ_f) of the molecules was determined using the following equation,

$$\Phi_f = \Phi_R I_S OD_R \eta_S^2 / I_R OD_S \eta_R^2 \tag{1}$$

where, Φ_f, I_S, OD_S, η_S are the fluorescence quantum yield, photoluminescence integrated areas, optical densities of the excitation wavelength, refractive indexes of sample respectively, and Φ_R, I_R, OD_R, η_R fluorescence quantum yield (9,10-diphenylanthracene; Φ_R = 0.95 in ethanol was used), photoluminescence integrated areas, optical densities of the excitation wavelength, refractive indexes of standard reference material respectively. The electrochemical stability was determined by cyclic voltammetry (CV) using a bio-logic (SP-50) potentiostat in degassed dichloromethane solution. Tetrabutylammoniumhexafluorophosphate (TBAPF$_6$: 0.1 M) was utilized as supporting electrolyte. The redox peak potential was obtained at the scan rate of 0.1 V s^{-1}. These was a three-electrode cell setup configuration which consist of platinum wire as an auxiliary electrode, a saturated Ag/Ag$^+$ reference electrode, platinum as a working electrode and ferrocene–ferrocenium ion (Fc/Fc$^+$) used as internal standard (4.8 eV). However, the onset potential was investigated at the intersect point of two tangents at the maximum slope of the photocurrent and background current of the cyclic voltammogram. Thermal behaviour of TGA and DSC were evaluated (T_d and T_g) under a nitrogen atmosphere at a heating rate of 10 °C min^{-1}.

Synthesis of BIMP-Br

A mixture of benzil (1 mmol), *p*-bromobenzaldehyde or 5-bromo-2-thiophene carboxaldehyde (1 mmol), *p*-anisidine (4 mmol) and NH$_4$OAc (4 mmol) was dissolved in glacial acetic acid (15 ml) and refluxed for 3 h under nitrogen atmosphere. The reaction was monitored using TLC after completion of the reaction it was cooled to room temperature and poured into ice water to precipitate. The precipitate was filtered and washed with 50 ml of water (four times), dried *in vacuo* and the crude product was further purified by column chromatography using silica gel (100–200 mesh), (hexanes/ethyl acetate; 4 : 2 v/v) to provide corresponding product as a white solid; yield: 5.2 g (75%); mp 188–190 °C; ¹H NMR (400 MHz, CDCl$_3$) δ: 7.75 (d, 2H, *J* = 4.0 Hz), 7.38–7.11 (m, 12H), 6.94 (d, 2H, *J* = 8.0 Hz), 6.76 (d, 2H, *J* = 8.0 Hz), 3.76 (s, 3H) ppm; ¹³C NMR (100 MHz, CDCl$_3$) δ: 159.3, 145.9, 138.3, 134.3, 131.5, 131.3, 131.1, 130.5, 130.3, 129.6, 129.4, 128.4, 128.2, 128.1, 127.4, 126.7, 122.6, 114.4, 55.4 ppm.

Synthesis of BIMT-Br

Pale yellow solid; yield: 5 g (72%); mp 203–205 °C: ¹H NMR (400 MHz, CDCl$_3$) δ: 7.46 (d, 2H, *J* = 7.2 Hz), 7.26–7.01 (m, 11H), 6.83 (d, 2H, *J* = 8.0 Hz), 6.65 (d, 2H, *J* = 12 Hz), 3.63 (s, 3H) ppm; ¹³C NMR (100 MHz, CDCl$_3$) δ: 159.3, 145.9, 138.3, 134.3, 131.6, 131.5, 131.3, 131.1, 130.4, 130.3, 129.50, 129.46, 129.37, 128.44, 128.40, 128.23, 128.16, 128.11, 127.3, 126.7, 122.6, 114.4, 55.3 ppm.

Synthesis of BIBP-AL

In a 30 ml of flame-dried Schlenk-flask BIMP-Br or BIMT-Br (1 mmol) and 4-formphenyl boronic acid (1.1 mmol) was dissolved in 20 ml THF. To this solution, 10 ml of 2 N K$_2$CO$_3$ solution and tetrakis(triphenylphosphine)palladium (0.002 mmol) were added. The reaction mixture was stirred at room temperature under nitrogen atmosphere for 0.5 h after that heated to 80 °C and kept for 12 h at the same temperature. The reaction was monitored using TLC after completion of the reaction cooled to room temperature and diluted with 50 ml of water. The reaction mixture was extracted with dichloromethane solution (2 × 50 ml), washed with water, dried over Na$_2$SO$_4$ and solvent removed under reduced pressure. The resultant residue was purified using column chromatography using silica gel (100–200 mesh) (hexanes/DCM, 7 : 3, v/v) to obtain corresponding product; yellowish white solid; yield: 1.5 g (71%); mp 227–228 °C; ¹H NMR (400 MHz, CDCl$_3$) δ: 9.98 (s, 1H), 7.87 (d, 2H, *J* = 8 Hz) 7.69–7.49 (m, 8H), 7.25–7.12 (m, 8H), 6.99 (d, 2H, *J* = 8.8 Hz), 6.76 (d, 2H, *J* = 12 Hz), 3.73 (s, 3H) ppm; ¹³C NMR (100 MHz, CDCl$_3$) δ: 191.9, 159.3, 146.3, 146.3, 139.0, 138.5, 135.3, 134.5, 131.6, 131.2, 130.8, 130.6, 130.3, 129.8, 129.5, 129.3, 128.5, 128.3, 128.1, 127.5, 127.4, 127.1, 126.7, 114.4, 55.4 ppm.

Synthesis of BIPT-AL

Pale yellow solid; yield: 1.2 g (57%); mp 212–213 °C; ¹H NMR (400 MHz, CDCl$_3$) δ: 9.94 (s, 1H), 7.82 (d, 2H, *J* = 8.4 Hz), 7.66 (d, 2H, *J* = 8 Hz), 7.59 (d, 2H, *J* = 7.2 Hz) 7.26–7.13 (m, 11H), 6.87 (d, 2H, *J* = 8.8 Hz), 6.60 (d, 1H, *J* = 4 Hz), 3.80 (s, 3H) ppm; ¹³C NMR (100 MHz, CDCl$_3$) δ: 191.4, 160.0, 142.6, 141.9, 139.7, 138.6, 135.1, 134.8, 134.1, 131.9, 131.0, 130.5, 130.1, 130.0, 129.0, 128.5, 128.2, 128.2, 127.4, 126.9, 126.8, 125.8, 125.4, 114.7, 55.5 ppm.

Synthesis of BIPIAN

In oven-dried round bottom flask BIBP-AL or BIPT-AL (1 mmol), indole-3-acetonitrile (1 mmol), and potassium *tert*-butoxide (2 mmol) were dissolved in dry methanol and refluxed at 70 °C. The reaction was monitored using TLC, after completion of the reaction mixture was cooled to room temperature and poured into ice water to give yellow precipitate and that was filtered and washed with water (2 × 25 ml) and methanol (1 × 25 ml) and again washed with water (1 × 25 ml). Then, the crude product was purified using column chromatography (silica gel 100–200 mesh) in hexanes : CH$_2$Cl$_2$ (4 : 2 v/v) as an eluent to obtain corresponding products. Greenish yellow solid; yield: 800 mg (63%); mp 253–254 °C; IR (neat): ν_{max} 2918, 2850, 1599, 1509, 1443, 1249, 1133, 1026, 822, 731 cm^{-1}; ¹H NMR (400 MHz, CDCl$_3$) δ: 11.76 (s, 1H), 8.10–8.00 (m, 3H), 7.86–7.73 (m, 6H), 7.54–7.51 (m, 5H), 7.32–7.19 (m, 12H), 6.91–6.90 (m, 2H), 3.73 (s, 3H) ppm; ¹³C NMR (100 MHz, DMSO-d$_6$) δ: 159.0, 145.6, 139.6, 138.5, 137.2, 136.9, 135.7, 134.4, 134.0, 131.8, 131.1, 130.5, 129.90, 129.86, 129.3, 129.1, 128.6, 128.44, 128.38, 128.1,

126.74, 126.68, 126.4, 126.32, 126.27, 123.6, 122.5, 120.5, 119.5, 118.5, 114.3, 112.4, 110.8, 105.5, 55.3 ppm; HRMS (ESI): $C_{45}H_{32}N_4O$ $[M + H]^+$ calcd m/z: 645.2654 obtained 645.2645.

Synthesis of BITIAN

Greenish yellow solid; yield: 950 mg (73%); mp 245–246 °C; IR (neat): ν_{max} 3055, 2926, 2212, 1650, 1511, 1439, 1247, 1113, 1025, 776 cm^{-1}; ^{1}H NMR (400 MHz, CDCl$_3$) δ: 11.78 (s, 1H), 8.09–7.76 (m, 7H), 7.52–7.19 (m, 17H), 7.0–6.98 (m, 2H), 6.35–6.34 (m, 1H), 3.78 (s, 3H) ppm; ^{13}C NMR (100 MHz, CDCl$_3$) δ: 159.6, 142.6, 141.2, 137.2, 136.9, 135.5, 134.0, 133.7, 133.1, 131.9, 131.0, 130.2, 130.0, 129.2, 128.53, 128.48, 128.2, 126.8, 126.6, 126.3, 126.0, 125.4, 125.0, 123.6, 122.5, 120.5, 119.5, 118.5, 114.6, 112.5, 110.8, 105.5, 55.4 ppm; HRMS (ESI): $C_{43}H_{30}N_4OS$ $[M + H]^+$ calcd m/z: 651.2219 obtained 651.2218.

Device fabrication and measurements

The electroluminescence device was fabricated on a glass substrate which is pre-coated with indium tin oxide (ITO) as anode, 1,4-bis[(1-naphthyl-phenyl)amino]biphenyl (NPB 40 nm) as a hole-transporting layer and 2,2′,2″-(1,3,5-benzinetriyl)-tris(1-phenyl-1-H-benzimidazole) (TPBi 20 nm) as electron transporting layer and lithium fluoride (LiF/Al) and aluminium used as bi-layer cathode, which are commercially available materials. Before using the device, the substrate was washed systematically and treated with oxygen plasma for 5 min and drying with air for 20 min at 150 °C. The hole transporting material (NPB) was vacuum deposited on cleaned ITO-coated glass substrate in nitrogen atmosphere for 20 min. Before making device, the emitter was treated at 100 °C under vacuum. Moreover, the emissive layer was thermally evaporated under nitrogen atmosphere for 20 min. Subsequently, TPBI and LiF/Al were successfully evaporated on emissive layer by vacuum thermal process. The device performance was carried out at ambient temperature with nitrogen atmosphere under dark place. The electrical behaviour of the device was used to analyse current density–voltage–luminescence by Minolta CS-1000 spectrometer and a Keithley 2400 source measuring system used to determine the OLED performance.

Computational details

All calculations have been performed using Gaussian 09.[48] The ground-state geometries of the considered molecules were fully optimized at DFT at B3LYP/6-31+G(d,p) level of theory.[49] The excited state geometries were fully optimized using *ab initio* configuration interaction singles method (CIS).[15,17] The vibrational frequency analysis of the optimized geometries confirms that all the optimized geometries are found to be minima on the potential energy surface with all real frequencies. The electronic absorption and emission spectra, both in vacuum and in solution, were systematically investigated by TD-DFT method at CAM-B3LYP/6-31+G(d,p) level.[50] The solvent effect has been included by the polarized continuum model (PCM).[51]

Conflicts of interest

There are no conflicts to declare.

Acknowledgements

References

1 J. Cornil, D. Beljonne, J. P. Calbert and J. L. Brédas, *Adv. Mater.*, 2001, **13**, 1053–1067.

2 M. Albota, D. Beljonne, J.-L. Brédas, J. E. Ehrlich, J.-Y. Fu, A. A. Heikal, S. E. Hess, T. Kogej, M. D. Levin, S. R. Marder, D. McCord-Maughon, J. W. Perry, H. Röckel, M. Rumi, G. Subramaniam, W. W. Webb, X.-L. Wu and C. Xu, *Science*, 1998, **281**, 1653–1656.

3 S. R. Forrest, *Nature*, 2004, **428**, 911.

4 C. W. Tang, *Appl. Phys. Lett.*, 1986, **48**, 183–185.

5 J. Mei, Y. Diao, A. L. Appleton, L. Fang and Z. Bao, *J. Am. Chem. Soc.*, 2013, **135**, 6724–6746.

6 C. W. Chu, J. Ouyang, J.-H. Tseng and Y. Yang, *Adv. Mater.*, 2005, **17**, 1440–1443.

7 P. N. Prasad and D. J. Williams, *Introduction to Nonlinear Optical Effects in Molecules and Polymers*, Wiley, New York, 1991.

8 Z.-Z. Lu, R. Zhang, Y.-Z. Li, Z.-J. Guo and H.-G. Zheng, *J. Am. Chem. Soc.*, 2011, **133**, 4172–4174.

9 (*a*) K. Okamoto, I. Niki, A. Shvartser, Y. Narukawa, T. Mukai and A. Scherer, *Nat. Mater.*, 2004, **3**, 601; (*b*) J. H. Burroughes, D. D. C. Bradley, A. R. Brown, R. N. Marks, K. Mackay, R. H. Friend, P. L. Burns and A. B. Holmes, *Nature*, 1990, **347**, 539.

10 M. Pope, H. P. Kallmann and P. Magnante, *J. Chem. Phys.*, 1963, **38**, 2042–2043.

11 Q. Zhang, J. Li, K. Shizu, S. Huang, S. Hirata, H. Miyazaki and C. Adachi, *J. Am. Chem. Soc.*, 2012, **134**, 14706–14709.

12 C. W. Tang and S. A. VanSlyke, *Appl. Phys. Lett.*, 1987, **51**, 913–915.

13 (*a*) M. A. Baldo, S. Lamansky, P. E. Burrows, M. E. Thompson and S. R. Forrest, *Appl. Phys. Lett.*, 1999, **75**, 4–6; (*b*) B. Geffroy, P. le Roy and C. Prat, *Polym. Int.*, 2006, **55**, 572–582.

14 D. A. Pardo, G. E. Jabbour and N. Peyghambarian, *Adv. Mater.*, 2000, **12**, 1249–1252.

15 A. C. Grimsdale, K. Leok Chan, R. E. Martin, P. G. Jokisz and A. B. Holmes, *Chem. Rev.*, 2009, **109**, 897–1091.

16 C. Adachi, M. A. Baldo, M. E. Thompson and S. R. Forrest, *J. Appl. Phys.*, 2001, **90**, 5048–5051.

17 (a) V. Jankus, P. Data, D. Graves, C. McGuinness, J. Santos, M. R. Bryce, F. B. Dias and A. P. Monkman, *Adv. Funct. Mater.*, 2014, **24**, 6178–6186; (b) H. Uoyama, K. Goushi, K. Shizu, H. Nomura and C. Adachi, *Nature*, 2012, **492**, 234; (c) S. Y. Lee, T. Yasuda, H. Nomura and C. Adachi, *Appl. Phys. Lett.*, 2012, **101**, 093306.

18 L. S. Liao, K. P. Klubek and C. W. Tang, *Appl. Phys. Lett.*, 2004, **84**, 167–169.

19 (a) Y. Zhu, R. D. Champion and S. A. Jenekhe, *Macromolecules*, 2006, **39**, 8712–8719; (b) M. R. Bryce, *Adv. Mater.*, 1999, **11**, 11–23.

20 A. P. Kulkarni, X. Kong and S. A. Jenekhe, *Adv. Funct. Mater.*, 2006, **16**, 1057–1066.

21 (a) Y. Yuan, J.-X. Chen, F. Lu, Q.-X. Tong, Q.-D. Yang, H.-W. Mo, T.-W. Ng, F.-L. Wong, Z.-Q. Guo, J. Ye, Z. Chen, X.-H. Zhang and C.-S. Lee, *Chem. Mater.*, 2013, **25**, 4957–4965; (b) N. Nagarajan, G. Velmurugan, A. Prakash, N. Shakti, M. Katiyar, P. Venuvanalingam and R. Renganathan, *Chem.–Asian J.*, 2014, **9**, 294–304; (c) A. Verma, S. Joshi and D. Singh, *J. Chem.*, 2013, **2013**, 12; (d) Y. Zhang, S.-L. Lai, Q.-X. Tong, M.-Y. Chan, T.-W. Ng, Z.-C. Wen, G.-Q. Zhang, S.-T. Lee, H.-L. Kwong and C.-S. Lee, *J. Mater. Chem.*, 2011, **21**, 8206–8214; (e) Y. Yuan, J.-X. Chen, W.-C. Chen, S.-F. Ni, H.-X. Wei, J. Ye, F.-L. Wong, Z.-W. Zhou, Q.-X. Tong and C.-S. Lee, *Org. Electron.*, 2015, **18**, 61–69.

22 (a) G. Mu, S. Zhuang, W. Zhang, Y. Wang, B. Wang, L. Wang and X. Zhu, *Org. Electron.*, 2015, **21**, 9–18; (b) D. Kumar, K. R. J. Thomas, Y.-L. Chen, Y.-C. Jou and J.-H. Jou, *Tetrahedron*, 2013, **69**, 2594–2602; (c) Z.-Y. Wang, B. Liu, J.-W. Zhao, G.-L. Ruan, S.-L. Tao and Q.-X. Tong, *Org. Electron.*, 2018, **52**, 89–97; (d) S. S. Reddy, W. Cho, V. G. Sree and S.-H. Jin, *Dyes Pigm.*, 2016, **134**, 315–324; (e) S. Fan, J. You, Y. Miao, H. Wang, Q. Bai, X. Liu, X. Li and S. Wang, *Dyes Pigm.*, 2016, **129**, 34–42; (f) P. Wang, S. Fan, J. Liang, L. Ying, J. You, S. Wang and X. Li, *Dyes Pigm.*, 2017, **142**, 175–182.

23 N. Nagarajan, A. Prakash, G. Velmurugan, N. Shakti, M. Katiyar, P. Venuvanalingam and R. Renganathan, *Dyes Pigm.*, 2014, **102**, 180–188.

24 N. Miyaura and A. Suzuki, *Chem. Rev.*, 1995, **95**, 2457–2483.

25 S. Chalais, P. Laszlo and A. Mathy, *Tetrahedron Lett.*, 1985, **26**, 4453–4454.

26 H. Huang, Y. Wang, B. Wang, S. Zhuang, B. Pan, X. Yang, L. Wang and C. Yang, *J. Mater. Chem. C*, 2013, **1**, 5899–5908.

27 C. Li, J. Wei, J. Han, Z. Li, X. Song, Z. Zhang, J. Zhang and Y. Wang, *J. Mater. Chem. C*, 2016, **4**, 10120–10129.

28 (a) G. Paramaguru, R. V. Solomon, S. Jagadeeswari, P. Venuvanalingam and R. Renganathan, *Eur. J. Org. Chem.*, 2014, 753–766; (b) P. Ganesan, V. S. Rajadurai, J. Sivanadanam, V. Ponnambalam and R. Rajalingam, *J. Photochem. Photobiol., A*, 2013, **271**, 31–44.

29 C. Reichardt, *Chem. Rev.*, 1994, **94**, 2319–2358.

30 N. Zhou, S. Wang, Y. Xiao and X. Li, *Chem.–Asian J.*, 2018, **13**, 81–88.

31 A. Molski, J. Hofkens, T. Gensch, N. Boens and F. De Schryver, *Chem. Phys. Lett.*, 2000, **318**, 325–332.

32 J. Lakowicz, *Principles of Fluorescence Spectroscopy*, Kluwer Academic/Plenum Publishers, New York, Boston, Dordrecht, London, Moscow, 1999.

33 (a) G. Velmurugan, S. A. Vedha and P. Venuvanalingam, *RSC Adv.*, 2014, **4**, 53060–53071; (b) G. Velmurugan, B. K. Ramamoorthi and P. Venuvanalingam, *Phys. Chem. Chem. Phys.*, 2014, **16**, 21157–21171; (c) G. Velmurugan and P. Venuvanalingam, *Dalton Trans.*, 2015, **44**, 8529–8542.

34 (a) M. A. De Oliveira, H. A. Duarte, J.-M. Pernaut and W. B. De Almeida, *J. Phys. Chem. A*, 2000, **104**, 8256–8262; (b) N. Nagarajan, G. Velmurugan, G. Prabhu, P. Venuvanalingam and R. Renganathan, *J. Lumin.*, 2014, **147**, 111–120; (c) N. Nagarajan, G. Velmurugan, P. Venuvanalingam and R. Renganathan, *J. Photochem. Photobiol., A*, 2014, **284**, 36–48; (d) R. Jagadeesan, G. Velmurugan and P. Venuvanalingam, *RSC Adv.*, 2016, **6**, 44569–44577; (e) S. Muruganantham, N. Nagarajan, G. Velmurugan, A. Prakash, M. Katiyar, P. Venuvanalingam and R. Renganathan, *Mater. Chem. Front.*, 2017, **1**, 1373–1383.

35 W. L. Jia, X. D. Feng, D. R. Bai, Z. H. Lu, S. Wang and G. Vamvounis, *Chem. Mater.*, 2004, **17**, 164–170.

36 C. H. Huang, F. Li and W. Huang, *Introduction to Organic Light-Emitting Materials and Devices*, Fudan University, Shanghai, 2005.

37 X. D. Liu, A. M. Ren, J. K. Feng, L. Yang, H. Xu, M. M. Shi and C. Sun, *Chem. Res. Chin. Univ.*, 2006, **27**, 2156–2159.

38 A. Tenderholt, *QMForge: A Program to Analyze Quantum Chemistry Calculations, Version 2.3.2*, http://qmforge.sourceforge.net.

39 R. V. Solomon, A. P. Bella, S. A. Vedha and P. Venuvanalingam, *Phys. Chem. Chem. Phys.*, 2012, **14**, 14229–14237.

40 (a) I. Litani-Barzilai, V. Bulatov, V. V. Gridin and I. Schechter, *Anal. Chim. Acta*, 2004, **501**, 151–156; (b) V. Lukeš, A. Aquino and H. Lischka, *J. Phys. Chem. A*, 2005, **109**, 10232–10238.

41 L. Y. Zou, A. M. Ren, J. K. Feng, Y. L. Liu, X. Q. Ran and C. C. Sun, *J. Phys. Chem. A*, 2008, **112**, 12172–12178.

42 A. J. Heeger, *Chem. Soc. Rev.*, 2010, **39**, 2354–2371.

43 (a) A. Curioni, M. Boero and W. Andreoni, *Chem. Phys. Lett.*, 1998, **294**, 263–271; (b) G. R. Hutchison, M. A. Ratner and T. J. Marks, *J. Am. Chem. Soc.*, 2005, **127**, 2339–2350.

44 K. Navamani, G. Saranya, P. Kolandaivel and K. Senthilkumar, *Phys. Chem. Chem. Phys.*, 2013, **15**, 17947–17961.

45 E. Badaeva, V. V. Albert, S. Kilina, A. Koposov, M. Sykora and S. Tretiak, *Phys. Chem. Chem. Phys.*, 2010, **12**, 8902–8913.

46 L.-Y. Zou, A.-M. Ren, J.-K. Feng and X.-Q. Ran, *J. Phys. Org. Chem.*, 2009, **22**, 1104–1113.

47 K. R. J. Thomas, J. T. Lin, Y.-T. Tao and C.-H. Chuen, *Chem. Mater.*, 2002, **14**, 3852–3859.

48 M. Frisch, G. Trucks, H. Schlegel, G. Scuseria, M. Robb, J. Cheeseman, G. Scalmani, V. Barone, B. Mennucci, G. Petersson, H. Nakatsuji, M. Caricato, X. Li, H. Hratchian, A. Izmaylov, J. Bloino, G. Zheng, J. Sonnenberg, M. Hada, M. Ehara, K. Toyota, R. Fukuda, J. Hasegawa, M. Ishida, T. Nakajima, Y. Honda, O. Kitao, H. Nakai, T. Vreven, J. Montgomery Jr, J. E. Peralta, F. Ogliaro, M. Bearpark, J. J. Heyd, E. Brothers, K. N. Kudin, V. Staroverov, R. Kobayashi, J. Normand, K. Raghavachari, A. Rendell, J. Burant, S. Iyengar, J. Tomasi, M. Cossi, N. Rega, N. Millam, M. Klene, J. E. Knox, J. B. Cross, V. Bakken, C. Adamo, J. Jaramillo, R. Gomperts, R. Stratmann, O. Yazyev, A. Austin, R. Cammi, C. Pomelli, J. Ochterski, R. L. Martin, K. Morokuma, V. Zakrzewski, G. Voth, P. Salvador, J. Dannenberg, S. Dapprich, A. Daniels, Ö. Farkas, J. Foresman, J. Ortiz, J. Cioslowski and D. Fox, *Gaussian 09, revision B. 01*, Gaussian, Inc., Wallingford, CT, 2010.

49 (*a*) A. D. Becke, *J. Chem. Phys.*, 1993, **98**, 5648–5652; (*b*) J. P. Perdew, *Phys. Rev. B: Condens. Matter Mater. Phys.*, 1986, **33**, 8822–8824; (*c*) A. D. Becke, *Phys. Rev. B: Condens. Matter Mater. Phys.*, 1988, **38**, 3098–3100; (*d*) C. Lee, W. Yang and R. G. Parr, *Phys. Rev. B: Condens. Matter Mater. Phys.*, 1988, **37**, 785–789.

50 (*a*) E. Runge and E. K. U. Gross, *Phys. Rev. Lett.*, 1984, **52**, 997–1000; (*b*) R. E. Stratmann, G. E. Scuseria and M. J. Frisch, *J. Chem. Phys.*, 1998, **109**, 8218–8224; (*c*) R. Bauernschmitt and R. Ahlrichs, *Chem. Phys. Lett.*, 1996, **256**, 454–464; (*d*) T. Yanai, D. P. Tew and N. C. Handy, *Chem. Phys. Lett.*, 2004, **393**, 51–57.

51 (*a*) M. Cossi, G. Scalmani, N. Rega and V. Barone, *J. Chem. Phys.*, 2002, **117**, 43–54; (*b*) E. Cances, B. Mennucci and J. Tomasi, *J. Chem. Phys.*, 1997, **107**, 3032–3041; (*c*) B. Mennucci and J. Tomasi, *J. Chem. Phys.*, 1997, **106**, 5151–5158.